Continuous Operation of Wind Power Plants Under Pole-to-Ground Fault in an HVDC System Consisting of Half-Bridge MMCs and Disconnecting Switches

Mitsuyoshi Enomoto, *Student Member, IEEE*, Kenichiro Sano, *Member, IEEE*, Junya Kanno, and Junichi Fukushima

***Abstract*—This article focuses on a multicircuit HVDC system which can localize the dc line fault without dc circuit breakers. The conventional fault clearing method causes the shutdown and the restart of the wind power plants, which results in the suspension of the power supply. The suspension may affect the balance of supply and demand, and may cause frequency drop in the onshore ac power system. To solve the problem, this article proposes a system switching method to enable the continuous operation of the wind power plants under the dc line fault. The proposed method utilizes the half-bridge modular multilevel converter to clear the fault while keeping the wind power plants operating. As a result, the proposed method realizes the continuous operation of wind power plants and shorten the transmission outage to 0.2 s. Thus, it greatly increases the supply reliability. Experimental results demonstrate the validity of the proposed method.**

***Index Terms*—DC line fault, HVDC transmission system, modular multilevel converters (MMC), system switching.**

I. Introduction

LARGE-SCALE offshore wind power plants (WPPs) require a transmission system under the sea with long-distance and large-capacity undersea cables. A high voltage dc (HVDC) transmission system is an option because it can reduce the cost [1]. In the North Sea, multiple point-to-point HVDC systems have been independently constructed in parallel for adjacent offshore WPPs in the same area [2]. Each point-to-point HVDC system has no redundancy for the dc line fault. Thus, the power transmission stops for a long time until the cable under the dc line fault is repaired.

To continue the power transmission under the dc line fault, a loop configuration is adopted to add redundancy to the dc transmission lines (HVDC grid). DC circuit breakers are often applied to the HVDC grid to clear the fault [3], [4]. Such system can continue the power transmission by way of the nonfaulted section after clearing the faulted section, which is selective fault clearing. There are some types of dc circuit breakers such as mechanical type [5], [6], solid-state type [7], [8], and hybrid type [9], [10], [11]. The hybrid type especially attracts attention because it combines the characteristics of the low loss of the mechanical type and the high-speed interruption of the solid-state type. A hybrid dc circuit breaker has been developed for Zhangbei ± 500-kV multiterminal HVDC system in China [12]. However, the system often requires a large number of dc circuit breakers as the system expands. DC circuit breakers are more complex and expensive than ac circuit breakers because they require a bulky current limiting inductor, surge arresters, and auxiliary devices to generate the zero point of dc current [13]. Therefore, the use of dc circuit breakers will increase the system cost. Furthermore, further studies are suggested for reliability, size reduction, and technical standards of dc circuit breakers for HVDC systems [14], [15].

There are some alternative methods to clear the dc line fault without dc circuit breakers [4]. Opening ac circuit breakers enables to stop the dc fault current from converters [16]. In addition to this, several fault-blocking converters have been proposed to interrupt the fault current. For example, a hybrid modular multilevel converter (MMC) which combines full-bridge cells and half-bridge cells can interrupt fault current at the dc side while compensating reactive power at the ac side [17], [18]. Besides this, MMCs consisting of various cells, such as a clamp double submodule [19], a switched-capacitor submodule [20], and other types [21], [22] have been proposed to block the dc fault. Thus, applying these methods to all the converter terminals enables a fault current to be cleared, which is nonselective fault clearing [3]. After that, dc disconnecting switches eliminate the faulted section, and the power transmission can be resumed by way of the nonfaulted sections. However, these methods cause the entire HVDC system to be suspended due to a fault [3]. Thus, they are not suitable for applying to a large-scale system. Features of the existing methods are summarized in Table I.

On the other hand, there is a multicircuit HVDC system which can avoid suspension of the entire system under dc fault without using dc circuit breakers [23]. This configuration separates the multiple dc circuits by the disconnecting switches and diodes. This enables to localize the dc line fault only in the single

Manuscript received 31 May 2022; revised 28 September 2022; accepted 15 November 2022. Date of publication 28 November 2022; date of current version 26 December 2022. This work was supported by the Japan Society for the Promotion of Science (JSPS) under KAKENHI Grant 18K04097 and Grant 21K04018. Recommended for publication by Associate Editor Z. Li. *(Corresponding author: Mitsuyoshi Enomoto.)*

Mitsuyoshi Enomoto and Kenichiro Sano are with the Department of Electrical and Electronic Engineering, Tokyo Institute of Technology, Tokyo 152–8552, Japan (e-mail: enomoto.m@pel.ee.e.titech.ac.jp; sano@ee.e.titech.ac.jp).

Junya Kanno and Junichi Fukushima are with the TEPCO Research Institute, Tokyo Electric Power Company Holdings, Yokohama 230-8510, Japan (e-mail: kanno.junya@tepco.co.jp; fukushima.junichi@tepco.co.jp).

Color versions of one or more figures in this article are available at https://doi.org/10.1109/TPEL.2022.3225209.

Digital Object Identifier 10.1109/TPEL.2022.3225209

TABLE I
FEATURES OF THE FAULT CLEARING METHODS

Fault clearing scheme	HVDC grid with dc circuit breakers (selective fault clearing)	HVDC grid with fault-blocking converters (non-selective fault clearing)	Multicircuit HVDC system with the proposed system switching
Suspension of power supply under a dc fault	No WPPs	Entire system	No WPPs
features	Further improvement is required in cost/reliability/size of dc circuit breakers	Applying to a large-scale system degrades the reliability	This realizes high reliability equivalent to the HVDC grid with dc circuit breakers

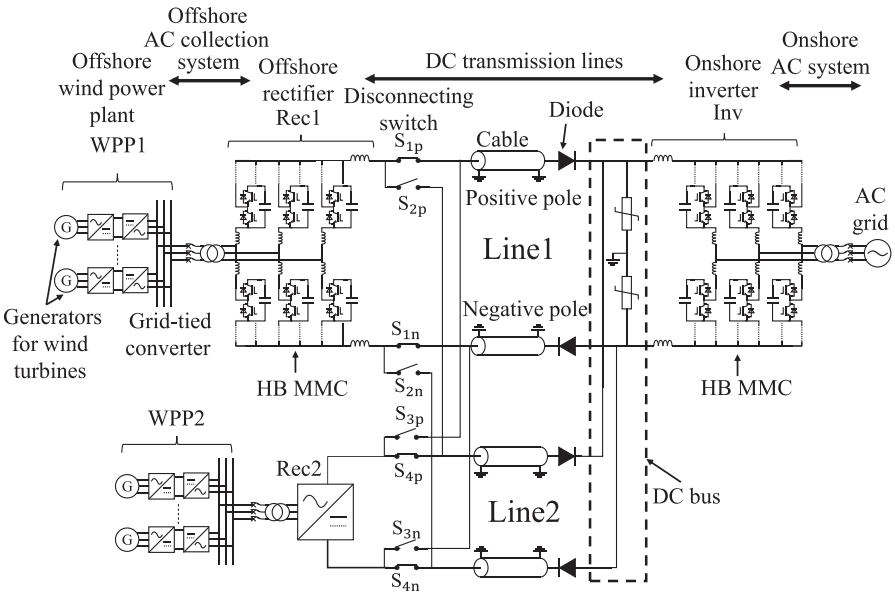

Fig. 1. Configuration of the double-circuit HVDC system.

circuit, and the other nonfaulted circuits can continue the power transmission. Therefore, the multicircuit HVDC system realizes the similar supply reliability as well as the HVDC grid with dc circuit breakers. However, the conventional fault clearing method still requires the shutdown of the WPPs in the faulted circuit. Even if the WPP is reconnected to the nonfaulted circuit by a system switching, the power transmission suspends until restarting the WPPs. The suspension of power transmission may affect the balance of supply and demand, and may cause frequency drop in onshore ac power system. In this article, we propose a system switching method that enables the continuous operation of WPPs under the dc line fault for the multicircuit HVDC system. The proposed method applies a new protection method to the half-bridge MMC (HB-MMC) for clearing the dc fault current. As a result, WPPs do not have to stop for fault clearing. All WPPs maintain their operation during the fault clearance and system switching from the faulted line to the nonfaulted line. Therefore, the proposed method greatly improves the supply reliability. The basic concept has been presented with the preliminary simulation results [24]. This article demonstrates the proposed method by experiments using a downscale system consisting of two 5.5-kW WPPs and HVDC transmission lines. Experimental results verify that the proposed method realizes the continuous operation of WPPs and reduces the time for resuming the power transmission to 0.2 s under the dc line fault.

II. CONFIGURATION OF THE MULTICIRCUIT HVDC SYSTEM

This section explains the configuration and control methods for the multicircuit HVDC system. Fig. 1 shows a configuration of the double-circuit HVDC system consisting of two dc transmission lines, which is for two offshore WPPs. The configuration can be extended to more than two by increasing the dc transmission lines, which is shown in Section II-D. The multicircuit HVDC system can be divided into three sections: 1) the offshore ac collection system; 2) the dc transmission lines; 3) the onshore ac grid. The ac power generated at the offshore WPPs (WPP1, WPP2) is collected by the ac collection system and converted to dc power by the offshore rectifiers (Rec1, Rec2). Then, the dc power is injected to the dc transmission line and received at the dc bus on the onshore side. The dc power is converted to ac power by onshore inverter (Inv) and injected into the onshore ac grid. Rec1, Rec2, and Inv apply the HB-MMC. Details of each section are described below.

A. Offshore ac Collection System

The offshore ac collection system applies the existing configuration and control method for WPPs [25]. The WPP consists of multiple generators for wind turbines and grid-tied converters. A fully rated back-to-back converter is applied to the grid-tied converter, and it connects the generator to the ac collection system. The offshore rectifier (Rec1, Rec2) controls the voltage

of the ac collection system to be constant amplitude and constant frequency. On the other hand, the grid-tied converters control their ac current to send the generated power to the ac collection system.

B. DC Transmission Lines

Each dc transmission line consists of two cables with the symmetrical monopole configuration, being composed of a positive pole of $+V_{\rm dc}/2$ and a negative pole of $-V_{\rm dc}/2$. In Fig. 1, two dc transmission lines, Line1 and Line2, are laid in parallel. At the sending end, the offshore rectifier Rec1 is equipped with two pairs of disconnecting switches ($\rm S_{1p}$, $\rm S_{1n}$) and ($\rm S_{2p}$, $\rm S_{2n}$). A pair of switches for the same line operates together. Two pairs ($\rm S_{1p}$, $\rm S_{1n}$) and ($\rm S_{2p}$, $\rm S_{2n}$) operate complementary, and the disconnecting switches connect the offshore rectifier to only one of the two transmission lines. For example, Rec1 is connected to Line1 ($\rm S_{1p}$ and $\rm S_{1n}$ are closed), but disconnected from Line2 ($\rm S_{2p}$ and $\rm S_{2n}$ are opened) in Fig. 1. Rec2 is also equipped with two pairs of disconnecting switches ($\rm S_{3p}$, $\rm S_{3n}$) and ($\rm S_{4p}$, $\rm S_{4n}$) as well as Rec1. But they are omitted in the following figures for their simplicity. The disconnecting switches operate after clearing the dc line fault, which is explained in the Section IV.

At the receiving end, two transmission lines are connected to the dc bus by way of diodes for blocking the fault current. Such blocking diodes have been applied to voltage-source inverters [26], [27], [28], whereas they are applied to the dc bus in this system. The diodes have to withstand the rated dc voltage to block the fault current. Thus, they generate some amount of conduction loss, whereas they are normally kept on-state and do not cause switching loss. Therefore, the calculated power loss is 0.02% [26] or 0.05% [27] of the transmission capacity, which is negligible comparing to the loss in the rectifiers and inverters. The dc bus is equipped with the braking chopper [29] to avoid overvoltage and also to balance the voltage between the positive pole and the negative pole of the symmetrical monopole configuration. The onshore Inv at the receiving end keeps the voltage of the dc transmission line constant. The offshore rectifiers (Rec1, Rec2) adjust the power flow by their dc current.

C. Onshore ac System

The onshore ac system is simplified as a voltage source in Fig. 1. The onshore Inv converts the dc power to ac. It controls its ac current to synchronize with the grid voltage. With the aforementioned controls, the entire system realizes power transmission from the WPPs to the onshore ac grid.

D. Extension of the Multicircuit HVDC System

The multicircuit HVDC system can be extended by increasing the WPPs and transmission lines. Fig. 2 shows the single-line diagram of the multicircuit HVDC system that connects six WPPs to an onshore ac system via three transmission lines. Each offshore rectifier is connected to either one of the two transmission lines by two pairs of disconnecting switches. All transmission lines are connected to the dc bus through diodes at the receiving end. Although the following sections explain the proposed method based on the double-circuit HVDC system, the same method is applicable to the extended configuration.

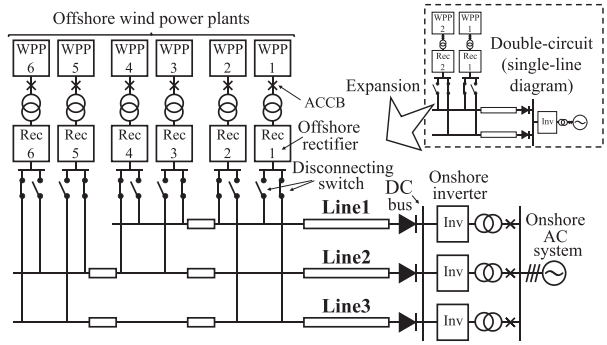

Fig. 2. Multicircuit HVDC system with six WPPs and three transmission lines.

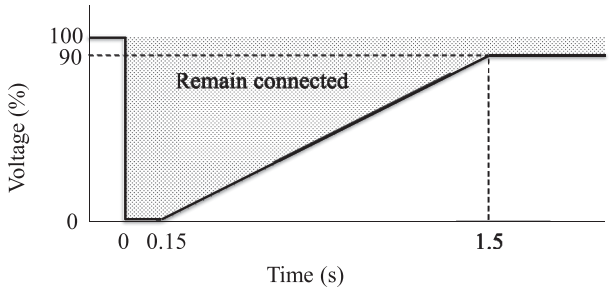

Fig. 3. Fault ride through requirement of wind power generations [33].

III. Strategy for the Continuous Operation of WPPs

The double-circuit HVDC system can resume the power transmission by applying system switching after fault clearance [23]. However, the previous method requires the shutdown of the WPP for clearing the fault. This happens because the fault is cleared by opening the ac circuit breaker, and no converter maintains the voltage of the ac collection system. The halted wind turbines stop rotation of their blades. To restart them, they gradually increase the rotation speed to the rated speed while adjusting the pitch angle of the blades. Because the restart coordinates with mechanical part, they cannot restart in a short time. Moreover, the capacity of a WPP reaches the scale of hundreds of megawatts [30]. Therefore, the suspension of the WPPs may cause frequency drop in the onshore ac system. Existing grid-tied converters for onshore WPPs are designed to comply with the grid code. The grid code includes the fault ride through (FRT) requirement for ac voltage sag. The FRT requirement contributes to prevent cascading dropout of the grid-tied converters by the voltage sag. Fig. 3 shows the Japanese FRT requirement for WPPs [33], which defines the fault conditions under which the WPPs continue their operation. WPPs that comply with the FRT requirement continue to operate against the voltage sag which continues 150 ms with the amplitude of 0% and recovers the amplitude to 90% over 1.5 s.

The proposed system switching method utilizes the FRT capability of the WPPs. The ability of FRT depends on the control of the WPPs. However, the WPP complying with the

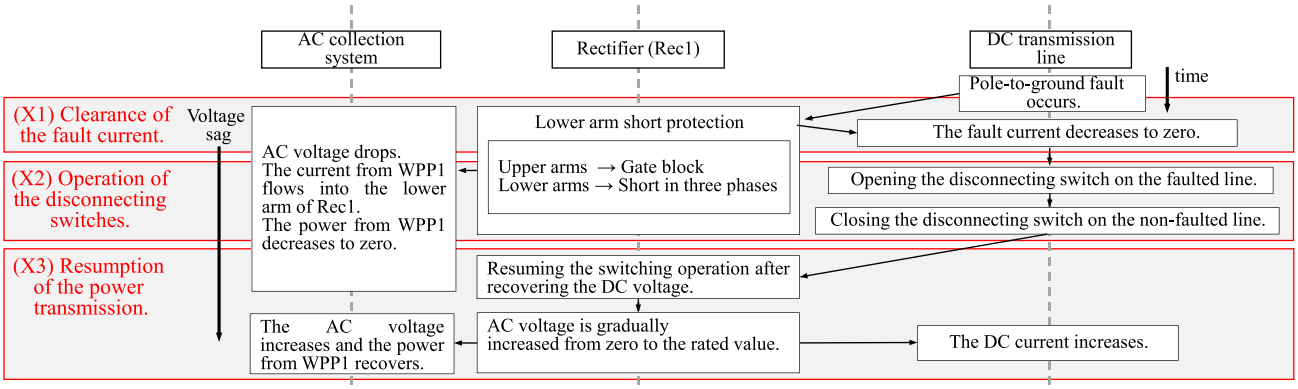

Fig. 4. Operating timelines of the system switching after the dc line fault.

FRT requirement should have the ability for the voltage sag specified in the grid code. The proposed method intentionally generates a voltage sag in the ac collection system during dc fault clearance and system switching. However, the voltage sag is designed to be minor to the FRT requirement. This can assure the WPPs to continue their operation.

At present, the FRT requirement is a regulation for onshore WPPs, and application to the offshore WPPs connected by an HVDC system is not mandatory. The proposed method imposes the same FRT requirement on the offshore WPPs. This means that the offshore WPPs can use the same control method as WPPs already in operation on land.

IV. Proposed System Switching Method Enabling the Continuous Operation of WPPs

This section explains the system switching method which enables the continuous operation of WPPs after the dc line fault (procedures X1–X3). In addition, this method is applicable during the normal operation. So this section also explains system switching in the normal operation (procedures Y1–Y3).

A. System Switching After the dc Line Fault (X1–X3)

The proposed system switching after the dc line fault consists of the following three procedures:

1) X1 Clearance of the fault current;
2) X2 Operation of the disconnecting switches;
3) X3 Resumption of the power transmission.

Fig. 4 shows the operating timelines of the proposed system switching. The vertical direction is the flow of time associated with the three procedures. Three timelines are associated with the operation of the ac collection system, the rectifier, and the DC transmission line, respectively. The following sections explain the method assuming that the line fault occurs on Line1 in Fig. 1. The same procedure is also applicable to Line2 because the system configuration is symmetrical.

Two types of fault are possible in the symmetrical monopole HVDC system: 1) pole-to-ground fault where either the positive or negative pole is grounded; 2) pole-to-pole fault where both poles are grounded. The undersea cables for the positive and negative poles are usually laid separately. Thus, pole-to-pole fault in undersea cables is rare compared to pole-to-pole fault in overhead lines. Therefore, this article focuses on the pole-to-ground fault for the target of the proposed method.

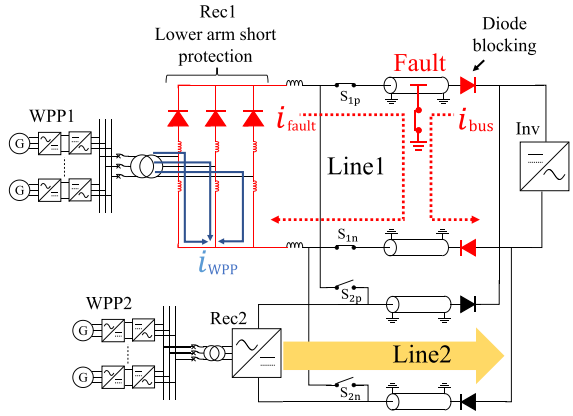

Fig. 5. Clearance of the fault current (X1).

1) Clearance of the Fault Current (X1): Fig. 5 shows the state during the clearance of the fault current. It assumes a positive pole-to-ground fault, but the same method can be applied to a negative pole-to-ground fault. When the pole-to-ground fault occurs at Line1, the fault current i_{bus} tries to flow into the fault point from the onshore inverter and the nonfaulted Line2 at the receiving end. The fault current i_{bus} is blocked by the blocking diodes installed between the transmission line and the dc bus. Therefore, the diodes suppress the spread of the fault at the receiving end. It enables the system to continue the power transmission from Rec2 using the nonfaulted Line2 as shown in Fig. 5.

At the sending end, the current i_{fault} flows into the fault point from Rec1. i_{fault} is blocked by the Rec1 which conducts the fault cleaning method called "lower arm short protection [31]" which was originally introduced to avoid the overvoltage in the symmetrical monopole configuration.

Fig. 6 shows the equivalent circuit of the lower arm short protection. Rec1 turns off all the switches of cells in the upper arms. On the other hand, the lower arms are bypassed by turning on the low-side switches of cells in the lower arms. Consequently,

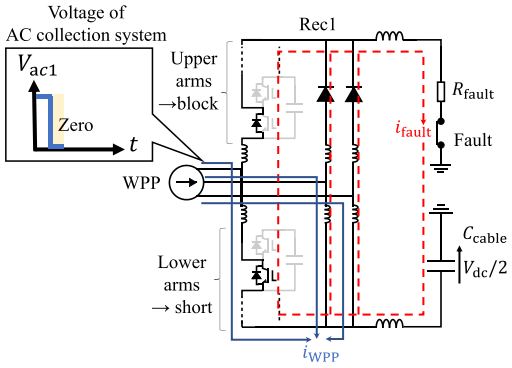

Fig. 6. Equivalent circuit of lower arm short protection.

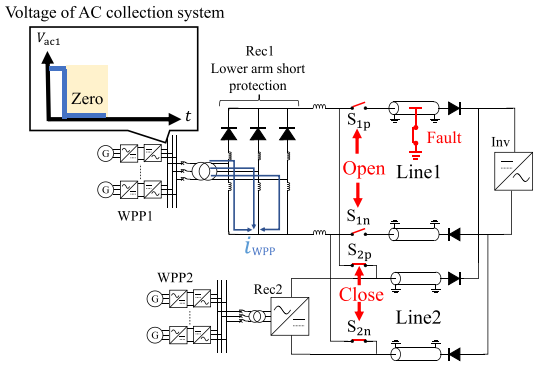

Fig. 7. Operation of the disconnecting switches (X2).

the lower arms form a short circuit among the three-phase ac terminals, and the voltage amplitude of the ac collection system V_{ac1} drops to almost zero as depicted in Fig. 6. At this time, the grid-tied converters of the WPP continue the current control and avoid their overcurrent. Therefore, WPP is represented by the current source of i_{WPP}. The current i_{WPP} circulates only in the shorted lower arms of Rec1, and it does not flow out to the dc side. On the other hand, the fault current i_{fault} flowing between Rec1 and the fault point starts the resonance among the dc inductors and the line-to-ground capacitance C_{cable} of the nonfaulted pole. C_{cable} holds the voltage of $V_{dc}/2$. The voltage decreases the fault current i_{fault}, and it is interrupted at the zero point by the diodes of the upper arm. Then, the diodes are reverse-biased by the residual voltage of C_{cable}. Therefore, the fault current is interrupted by the lower arm short protection at the sending end, while the WPP continues the operation and flows the current through the lower arm of the rectifier. As a result, the current amplitude during the lower arm short protection becomes 1.35–1.62 times larger than that of the normal operation (cf. Appendix A). The lower arms of the rectifier should be designed to withstand the current.

2) Operation of the Disconnecting Switches (X2): Fig. 7 shows the operation of the disconnecting switches. After the clearance of the fault current, Rec1 is disconnected from the faulted Line1 and connected to the nonfaulted Line2. First, the disconnecting switches S_{1p}, S_{1n} on the faulted Line1 are opened. At this time, the disconnecting switch does not need the current interrupting capability because the fault current has already been interrupted by the Rec1 with lower arm short protection. Next, the disconnecting switches S_{2p}, S_{2n} to the nonfaulted Line2 are closed. At this time, the voltage of the nonfaulted line V_{dc} is applied to Rec1. However, no inrush current flows because Rec1 continues the lower arm short protection and the diodes of the upper arm are reverse-biased.

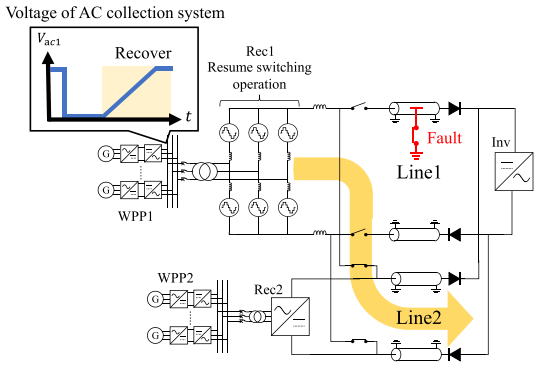

Fig. 8. Resumption of the power transmission (X3).

The Rec1 continues the lower arm short protection during the operation of the disconnecting switches. Although WPP1 keeps the current flowing, this current only circulates in the Rec1 which is shorted in three phases. Therefore, Rec1 does not receive any active power and maintains the voltages of the cell capacitors constant. On the other hand, the voltage amplitude of the ac collection system V_{ac1} remains almost zero, as depicted in Fig. 7.

3) Resumption of the Power Transmission (X3): Fig. 8 shows the state after resuming the power transmission. The Rec1 quits the lower arm short protection and restarts the switching operation. The Rec1 gradually increases the voltage of the ac collection system from zero to the rated value as depicted in Fig. 8. Thus, WPP1 resumes power supply to the Rec1 through the ac collection system. Then, the power transmission from the Rec1 to the Inv is resumed by way of the nonfaulted Line2.

By the above-mentioned operation, the power transmission can be resumed after clearing the line fault. On the other hand, the voltage sag occurs in the ac collection system during the operation. This voltage sag has to be designed to be minor to the FRT requirement so that the WPPs continue their operation.

B. Design of the System Switching Based on the FRT Requirement

During the system switching, the voltage sag occurs in the ac collection system as shown in Fig. 8. If this voltage sag is prolonged, the WPP connected to the ac collection system finally stops. To prevent that, the system switching is designed so that the voltage sag becomes minor compared to the FRT requirement and enables the continuous operation of the WPP.

1) Zero-Voltage Period: FRT requirement allows the zero-voltage period of 0.15 s as shown in Fig. 3. The offshore rectifier Rec1 outputs zero voltage during the lower arm short protection. It continues until the Rec1 is connected to the nonfaulted line. Therefore, the zero-voltage period t_{Zero} is approximately expressed as follows:

$$t_{Zero} \simeq t_{Int} + t_{Open} + t_{Close}$$

where $t_{\rm Int}$ is the time to interrupt the fault current by the lower arm short protection in the X1. $t_{\rm Open}$ and $t_{\rm Close}$ are opening time and closing time of disconnecting switches, respectively, in the X2.

$t_{\rm Int}$ can be estimated by the following procedure. During interrupting the fault current, the fault current $i_{\rm fault}$ flows in the equivalent circuit shown in Fig. 6. In this equivalent circuit, the transmission line is treated as a lumped constant and the discharge from capacitors excepting nonfaulted pole are ignored for simple consideration. As a result, the transition of $i_{\rm fault}$ depends on the resonance between the total inductance L of the transmission line and the inductor of the Rec1, the line-to-ground capacitance $C_{\rm cable}$, and the fault resistance $R_{\rm fault}$. Therefore, the transition of $i_{\rm fault}$ can be described as follows:

$$0 = L\frac{d}{dt}i_{\rm fault} + R_{\rm fault}i_{\rm fault} + \frac{1}{C_{\rm cable}}\int i_{\rm fault}dt.$$

This equation yields $i_{\rm fault}$ when $R_{\rm fault} < 2\sqrt{L/C_{\rm cable}}$ as follows:

$$i_{\rm fault}(t) = e^{-\frac{R_{\rm fault}}{2L}t}A\sin(B-\omega t)$$

where

$$\omega = \sqrt{\frac{1}{C_{\rm cable}L} - \left(\frac{R_{\rm fault}}{2\,L}\right)^2}$$

$$A = \sqrt{I_0^2 + \left(\frac{R_{\rm fault}I_0}{2\omega L} + \frac{V_0}{\omega L}\right)^2}$$

$$\tan B = \frac{2\omega L I_0}{2V_0 + R_{\rm fault}I_0}.$$

I_0 is the dc current when Rec1 starts the lower arm short protection, which is almost equal to the rated current $I_{\rm dc}$. V_0 is the residual voltage of $C_{\rm cable}$, which is almost equal to half the rated voltage $V_{\rm dc}/2$. $i_{\rm fault}$ is finally interrupted by the diodes when it reaches zero. Therefore, the interrupting time $t_{\rm Int}$ is obtained as follows:

$$i_{\rm fault}\left(t_{\rm Int}\right) = e^{-\frac{R_{\rm fault}}{2L}t_{\rm Int}}A\sin\left(B-\omega t_{\rm Int}\right) = 0$$

$$\therefore t_{\rm Int} = \frac{B}{\omega} = \frac{1}{\omega}\tan^{-1}\left(\frac{2\omega L I_0}{2V_0 + R_{\rm fault}I_0}\right)$$

$$= \frac{1}{\omega}\tan^{-1}\left(\frac{2\omega L I_{\rm dc}}{V_{\rm dc} + R_{\rm fault}I_{\rm dc}}\right).$$

For example, assuming a $\pm 400\,$kV symmetrical monopole HVDC system, the $t_{\rm Int}$ can be calculated as 0.5 ms referring to the following parameters of an XLPE undersea cable [32]: $V_{\rm dc}/2 = 400\,$kV, $I_{\rm dc} = 760\,$A, $\Delta L = 2 \times 1.4\,$mH/km, $\Delta C_{\rm cable} = 0.13\,\mu$F/km, $R_{\rm fault} = 0\,\Omega$, and the length of the cable l is 100 km (substitute $L = \Delta L \times l, C_{\rm cable} = \Delta C_{\rm cable} \times l$). In addition, Fig. 9 shows the variation of $t_{\rm Int}$ when changing the following: 1) cable length l (with $R_{\rm fault} = 0\,\Omega$); 2) fault resistance $R_{\rm fault}$ (with $l = 100\,$km). Although the value $t_{\rm Int}$ varies depending on l (fault location) or $R_{\rm fault}$, $t_{\rm Int}$ is on the order of several milliseconds. Thus, $t_{\rm Int}$ is much shorter than the operating times of disconnecting switches $t_{\rm Open}$, $t_{\rm Close}$ which are dozens of milliseconds. Therefore, there is little impact of the fault location or fault resistance, and the zero-voltage period $t_{\rm Zero}$ is determined mainly by $t_{\rm Open}$ and $t_{\rm Close}$.

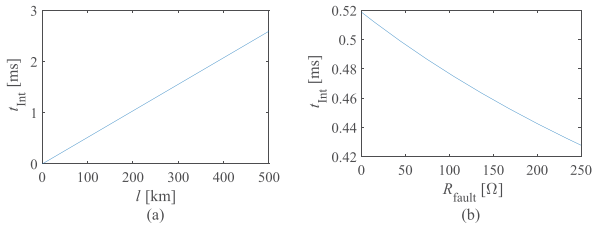

Fig. 9. Interruption time $t_{\rm Int}$ where changing (a) cable length l, or (b) fault resistance $R_{\rm fault}$.

In this article, $t_{\rm Open}$ and $t_{\rm Close}$ are set to 40 ms and 50 ms, respectively, based on the operating time of the existing ultra-high voltage (UHV) ac circuit breakers. Disconnecting switches can open only with zero current. Thus, after detecting zero current, the controller sends an open command to them. Therefore, the disconnecting switches start to open when the current reaches zero, and becomes completely isolated after about 40 ms. As a result, $t_{\rm Zero}$ becomes 90 ms ($\simeq t_{\rm Open} + t_{\rm Close}$), which has 60 ms margin for the zero-voltage period specified in the FRT requirements (150 ms).

2) Voltage Recovery Time: As shown in Fig. 3, the FRT requirement allows the voltage sag that returns to 90% in 1.5 s. The proposed method makes Rec1 recover the voltage of the ac collection system in the procedure X3. In this article, the voltage is raised over 0.1 s by the Rec1.

With these settings, the voltage sag while system switching recovers in 0.2 s, which is the sum of the zero-voltage period of 90 ms and the voltage recovery time of 0.1 s. Because this voltage sag is minor to the FRT requirement, the wind power plants can continue their operation over the voltage sag. As a result, power transmission can resume in 0.2 s.

C. System Switching in the Normal Operation (Y1–Y3)

The proposed system switching method is applicable not only after the dc line fault but also during the normal operation. Generally, a cable fault does not self-recover, and it is necessary to replace the faulted cable to resume power transmission. After repairing the cable, the system switching is carried out to change the connection of WPP1 and Rec1. The system switching moves them from Line2 to the recovered Line1 and returns to the state before the fault. The system switching is performed in the following three procedures:

1) Y1 Suspension of the power transmission;
2) Y2 Operation of the disconnecting switches;
3) Y3 Resumption of the power transmission.

A voltage sag occurs in the ac collection system during the system switching. Therefore, it is also designed based on the FRT requirement. As a result, the wind power plants can continue their operation during the system switching.

1) Suspension of the Power Transmission (Y1): First, Rec1 reduces the voltage of the ac collection system in a ramp shape from the rated value to zero to suspend the power transmission.

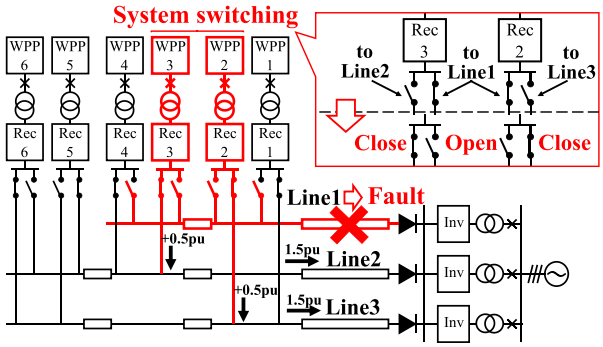

Fig. 10. System switching after the fault of Line1 in the triple-circuit HVDC system.

TABLE II
CIRCUIT PARAMETERS OF THE EXPERIMENTAL SETUP

Rated power of the rectifier		5.5 kW
Rated power of the inverter		13 kW
Rated value of the dc voltage		±170 V
Rated value of the ac voltage	V_s	200 V
The reference of the cell capacitor voltage		50 V
Inductance of the transmission line	L_{Cable}	0.5 mH
Earth capacitance of the transmission line	C_{Cable}	1 mF
Fault resistance	R_{Fault}	3.3 Ω
DC inductor of Rec1	L_{DC}	5.7 mH

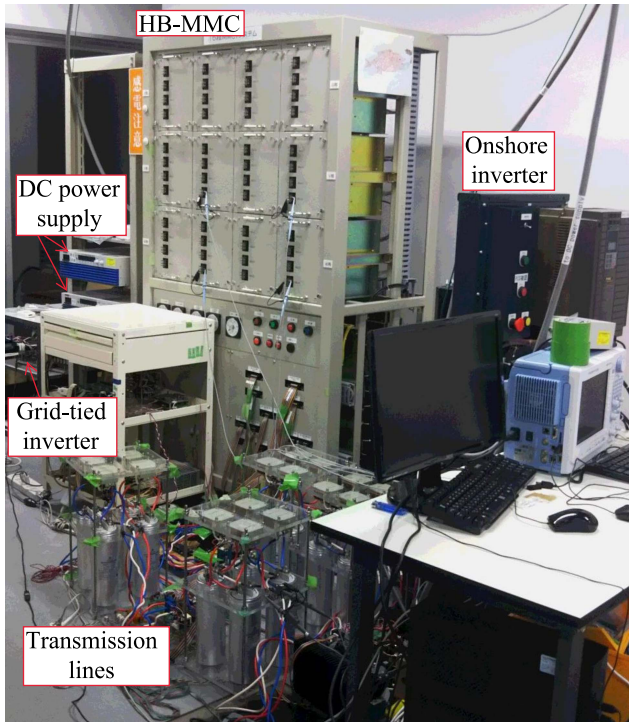

Fig. 11. Experimental setup.

The operation decreases the active power flow from WPP1 to Rec1. It also gradually decreases the dc current in the Rec1, resulting in mitigating the transient disturbance in the transmission system. The reference to dc current control is given by the feedforward of the active power flowing into Rec1 and the feedback control of cell capacitor voltages of Rec1.

Next, Rec1 starts the lower arm short protection to keep the dc current completely zero. The upper arms of Rec1 are blocked and the diodes of upper arms are reverse-biased by the line voltage. During the lower arm short protection, WPP1 flows its ac current through the lower arms of Rec1 and continues its operation. The ac current does not flow out to the ac terminal.

2) Operation of the Disconnecting Switches (Y2): The connection of Rec1 is changed from Line2 to Line1. The disconnecting switches (S_{2p}, S_{2n}) on the nonfaulted Line2 are opened, and the disconnecting switches on the recovered Line1 (S_{1p}, S_{1n}) are closed.

3) Resumption of the Power Transmission (Y3): Rec1 quits the lower arm short protection and restarts the switching operation. At this time, an inrush current may hinder the operation of Rec1 especially if the dc line is not precharged. To prevent the inrush current, Rec1 initially holds its ac voltage to be zero. As a result, the Rec1 can output an arbitrary dc voltage between zero and the rated value at its dc terminal. Therefore, the dc current control works effectively and avoids overcurrent due to the inrush current even if the recovered Line1 has no initial charge. Thus, the Rec1 can restart the operation regardless of the initial voltage of the recovered Line1.

After that, the dc line is charged to the rated voltage by the dc current of Rec1. Then, Rec1 raises its ac voltage from zero to the rated value in a ramp shape. The increase of the ac collection voltage resumes the power transmission from WPP1, resulting in the increase of the dc current. Then, the power transmission is resumed by way of the recovered Line1.

D. Cable Capacity for System Switching

The cable capacity depends on the number of transmission lines and the required transmission capacity after the fault. This section describes some cases as examples.

1) Double-Circuit System Requiring Rated Transmission Capacity After the System Switching: In the double-circuit system, all the WPPs are connected to the single circuit when one of the two circuits are disabled by a fault. To continue the fully rated power generation by WPPs, the cables in operation have to be designed to handle twice the capacity of normal operation. This case can realize high supply reliability, whereas it has to accept the high system cost.

2) Double-Circuit System Reducing Transmission Capacity After the System Switching: If the increase of cable capacity is not acceptable at all, it is necessary to operate with a reduced transmission capacity. There is also a benefit in the transmission systems for WPPs because the capacity factor of WPPs is relatively low. Thus, most of the time the cable transmits the power below its capacity. After system switching, the transmission capacity is limited within the capacity of the single circuit. Thus, the total output of WPPs must be curtailed within the capacity of the single circuit. This case can reduce the system cost, whereas sacrificing the supply reliability.

3) Triple-Circuit System Requiring Rated Transmission Capacity After the System Switching: In the triple-circuit configuration shown in Fig. 2, the required cable capacity for system

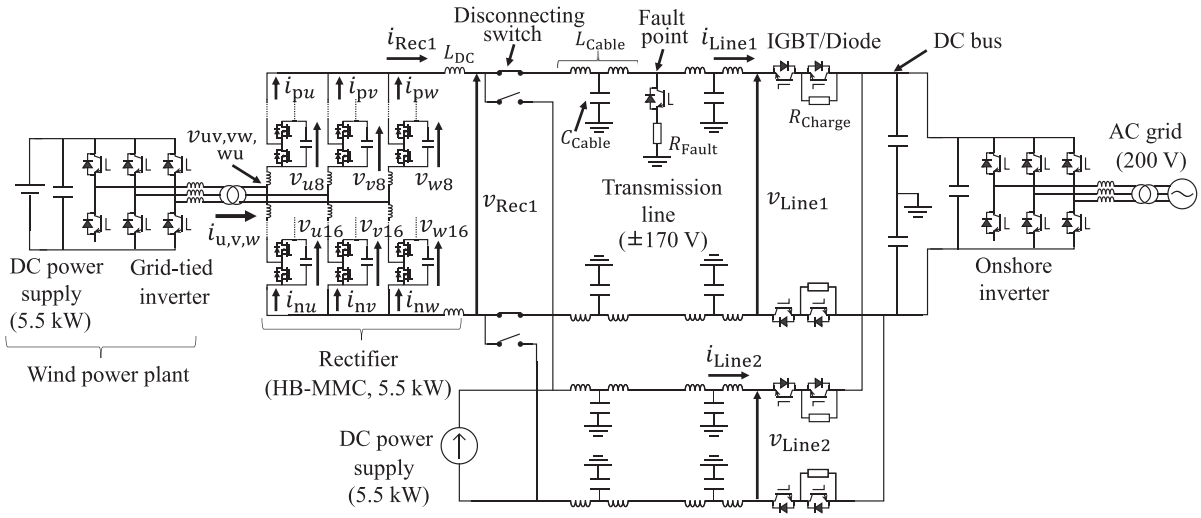

Fig. 12. Circuit diagram of the experimental setup.

switching can be reduced than the double-circuit configuration. When a fault occurs on Line1, Rec2, and Rec3 execute the system switching. WPP2 and Rec2 switch from the Line1 to the Line3, and WPP3 and Rec3 switch from the Line1 to the Line2 as shown in Fig. 10. As a result, both Line2 and Line3 increase their transmitted power 1.5 times larger capacity of normal operation, whereas the double-circuit system increases to twice the capacity of normal operation. Thus, the required cable capacity can be further reduced as the system is extended. This is because the power flow of the disabled circuit can be transferred to multiple circuits by the system switching.

V. Experimental Verification

Experiments were carried out to verify the system switching after the dc line fault (X1–X3) and in the normal operation (Y1–Y3). Fig. 11 shows the experimental setup and Fig. 12 shows the circuit diagram. Table II summarizes the circuit parameters. The setup is a downscaled double circuit system consisting of two 5.5-kW WPPs and two HVDC transmission lines. A pole-to-ground fault is simulated by an insulated gate bipolar transistor (IGBT) switch inserted between the neutral point and the positive pole of the Line1. WPP1 is simply modeled by a dc power supply (constant voltage mode) and a two-level grid-tied inverter. The grid-tied inverter is connected to Rec1 by way of a transformer, and injects the rated power of 5.5 kW. Rec1 is a HB-MMC with eight half-bridge cells in each arm. The Rec1 converts the ac power to the dc and injects the dc power into the transmission line. Two contactors are used for simulating the disconnecting switches beside the Rec1.

WPP2 and Rec2 are simplified by the dc power supply in constant current mode because they are connected to the nonfaulted Line2. The dc transmission lines are modeled by a T-shaped equivalent circuit. According to the physical layout of a 1.5-GW ±500-kV single-core XLPE cable, line impedances for the lumped constant circuit model were extracted by a line constants calculation program. The line impedances were scaled down for an 11-kW and ±170-V experimental system.

DC power from the two transmission lines is converted to the ac power by the two-level onshore inverter and injected into the ac system. The onshore inverter controls the dc voltage of the transmission line at the rated value of 340 V.

Because of the diodes on dc bus, power cannot flow from the onshore inverter to the offshore rectifier. However, additional switches temporarily enable the reverse power flow as shown in [28]. For precharging the transmission line and starting up the rectifier, IGBT switches and charging resistors R_{Charge} are inserted between the dc bus and the transmission line. The IGBT switches are ON-state only during precharge. Then, they are turned OFF during the experiment to operate them as diodes for blocking the fault current. If the start-up method from onshore side is not applicable, the rectifier and the WPP can also start up by using auxiliary power supply for their black start.

A. System Switching After the dc Line Fault (X1–X3)

Fig. 13 shows the experimental result of the proposed system switching method under the pole-to-ground fault, where each value is shown by the per-unit value using the rated value for its base. Initially, Rec1 was connected to Line1 and each of the two transmission lines supplied 5.5-kW power. Then, the IGBT switch at Line1 caused the pole-to-ground fault at 0 s. The operation of system switching is confirmed in the sequence of the procedures X1–X3.

1) Clearance of the Fault Current (X1): When the pole-to-ground fault occurs at time $t = 0$ s, the voltage of Line1 v_{Line1} dropped to 0.5 pu. DC line current i_{Line1} indicates that the fault current from the dc bus was immediately blocked. This was the effect of the diodes installed between the dc bus and the Line1.

At the sending end, Rec1 conducted the lower arm short protection after detecting the drop in dc voltage v_{Rec1}. The dc current of Rec1 i_{Rec1} immediately decreased to zero because the residual voltage of 0.5 pu in v_{Rec1} was applied to Rec1. i_{Rec1}

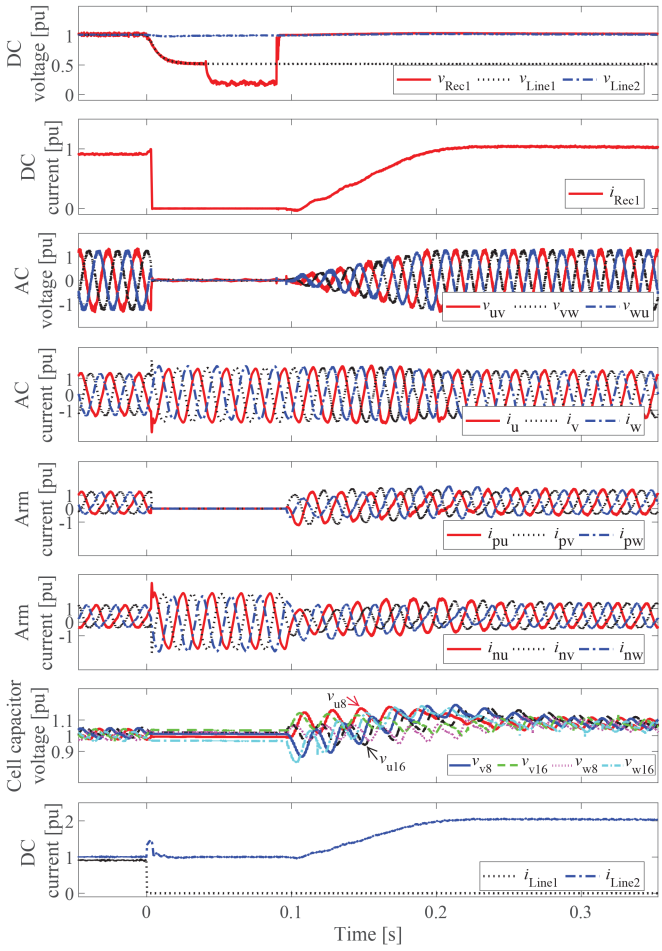

Fig. 13. Experimental result of the system switching from the faulted Line1 to the nonfaulted Line2 under the pole-to-ground fault (X1–X3).

was kept at zero by the reverse-biased diodes of the upper arms in Rec1. The voltages of the ac collection system v_{uv}, v_{vw}, v_{wu} dropped to almost zero because the short-circuit was created in the three-phase ac terminals by the lower arm short protection. At this time, the grid-tied inverter controlled the ac currents i_{u}, i_{v}, i_{w} to the rated value without causing overcurrent against the voltage sag. The currents flowed only through the lower arms of Rec1 as seen from i_{nu}, i_{nv}, i_{nw}, and they did not flow out to the ac side as seen from i_{Rec1}. As a result, both i_{Rec1} and i_{Line1} were kept at zero. This means that the fault current was interrupted with the operation.

2) Operation of the Disconnecting Switches (X2): The connection of Rec1 was changed from the faulted Line1 to the nonfaulted Line2 by the disconnecting switches. When the dc current i_{Rec1} reached zero, the controller opened the disconnecting switch on the faulted Line1. The switch opened after the delay of 40 ms to mimic the actual high-speed disconnecting switch. After opening the disconnecting switch, the controller closed the disconnecting switch on the nonfaulted Line2. The switch was closed after a delay of 50 ms. While this operation was carried out, Rec1 continued the lower arm short protection and the voltages of the ac collection system v_{uv}, v_{vw}, and v_{wu} were kept almost zero. Therefore, Rec1 did not receive any active

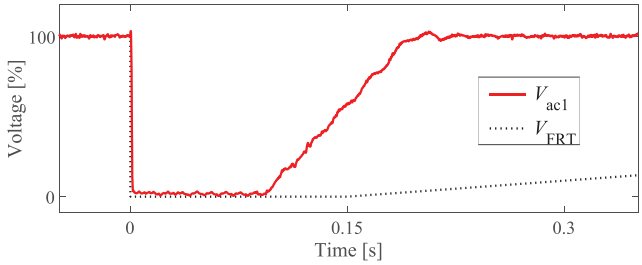

Fig. 14. Comparison of the experimental result with the FRT requirement in the case of the system switching after the dc line fault (X1–X3).

power, while the currents of WPPs i_{u}, i_{v}, and i_{w} continued to flow through Rec1 as seen in i_{nu}, i_{nv}, and i_{nw}. The cell capacitor voltages of Rec1 v_{u8}, v_{v8}, v_{w8}, v_{u16}, v_{v16}, v_{w16}, were kept constant.

3) Resumption of the Power Transmission (X3): When Rec1 was connected to the nonfaulted Line2 at $t = 90$ ms, the voltage of the Line2 was imposed to the Rec1, and the dc voltage v_{Rec1} rose to the rated value. After detecting the voltage rise, Rec1 quit the lower arm short protection and restarted the switching operation. The ac voltage was raised in a ramp shape over 100 ms as shown in v_{uv}, v_{vw}, v_{wu}. This operation resumed the power flow from WPP1 to Rec1, which also increased the dc current of Rec1 i_{Rec1} to the rated value at $t = 0.2$ s. The cell capacitor voltages of Rec1 v_{u8}, v_{v8}, v_{w8}, v_{u16}, v_{v16}, v_{w16} were well balanced against the disturbance.

The currents of Line1 i_{Line1} and Line2 i_{Line2} were 1 pu each before the fault ($t < 0$ s). Then, i_{Line1} decreased to 0 pu when the fault occurred in Line1 at $t = 0$. After the system switching ($t > 0.2$ s), i_{Line2} increased to 2 pu. This result demonstrates that the power transmission of Line1 was transferred to Line2 by the system switching in 0.2 s.

4) Comparison With the FRT Requirement (X1–X3): Fig. 14 shows the voltage amplitude of the ac collection system V_{ac1}, and the FRT requirement V_{FRT}. V_{ac1} is the amplitude of the space vector of v_{uv}, v_{vw}, v_{wu}, which was obtained by the $\alpha\beta$ conversion and a low-pass filter to remove the switching ripple. V_{ac1} dropped when Rec1 conducted the lower arm short protection, but it recovered to the rated value in 0.2 s as designed in the Section IV-B. This voltage sag is within the range for continuous operation in the FRT requirement. Therefore, the WPPs will be able to continue their operation against the voltage sag caused by the proposed system switching.

Therefore, the experimental results verify that the proposed method reduces the time for resuming the power transmission to 0.2 s under the dc line fault with the continuous operation of WPPs.

B. System Switching in the Normal Operation (Y1–Y3)

Fig. 15 shows the experimental result of the system switching in the normal operation. At first, Rec1 was connected to the nonfaulted Line2 by the system switching after the fault in Line1. The initial voltage of the recovered Line1 v_{Line1} was zero.

1) Suspension of the Power Transmission (Y1): First, Rec1 decreased its ac voltages v_{uv}, v_{vw}, v_{wu} over 20 ms, resulting

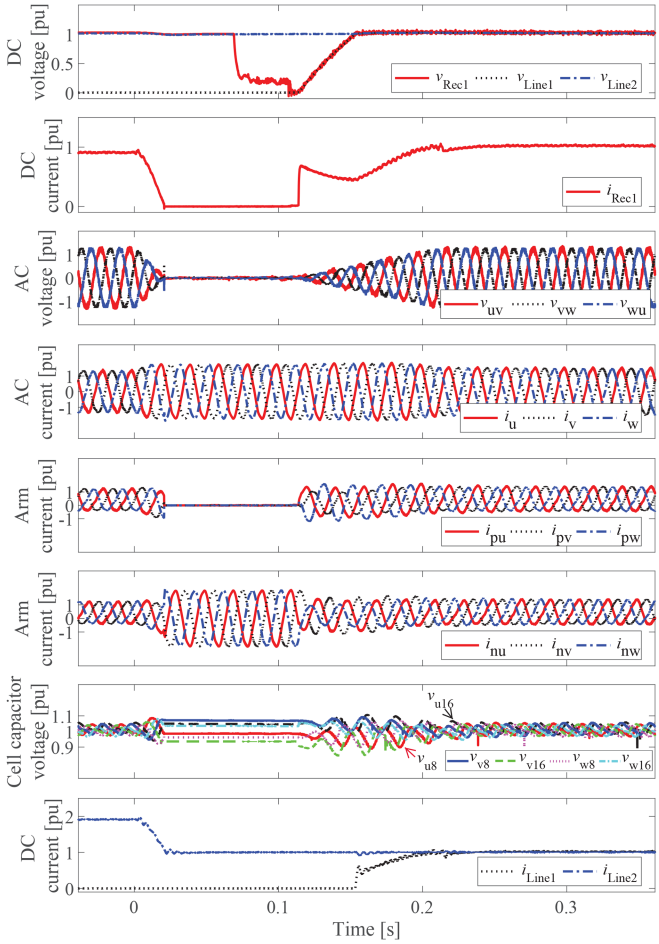

Fig. 15. Experimental result of the system switching from Line2 to uncharged Line1 in the normal operation (Y1–Y3).

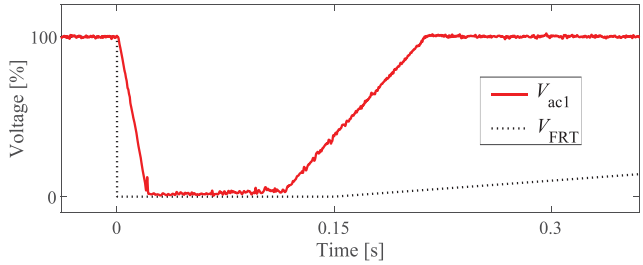

Fig. 16. Comparison of the experimental result with the FRT requirement in the case of the system switching in the normal operation (Y1–Y3).

in the decrease of the active power flow from the WPPs to the Rec1. Then, the dc current i_{Rec1} decreased by the current control. After the ac voltages $v_{\mathrm{uv}}, v_{\mathrm{vw}}, v_{\mathrm{wu}}$ reached zero, Rec1 conducted lower arm short protection at $t = 0.02$ s. As a result, i_{Rec1} was interrupted because the diodes of upper arms were reverse biased by the voltage of the nonfaulted line v_{Line2}.

2) Operation of the Disconnecting Switches (Y2): Then, the disconnecting switch on the nonfaulted Line2 was opened with the operation delay of 40 ms, and the disconnecting switch on the recovered Line1 was closed with the delay of 50 ms, which can be confirmed by the dc voltage v_{Rec1}.

3) Resumption of the Power Transmission (Y3): At $t = 0.115$ s, Rec1 stopped the lower arm short protection and restarted the switching operation. The dc current i_{Rec1} started to flow and the voltage of the recovered Line1 v_{Line1} increased from zero to the rated value. Inrush current in i_{Rec1} was suppressed by the current control of Rec1.

Then, Rec1 raised its ac voltages $v_{\mathrm{uv}}, v_{\mathrm{vw}}, v_{\mathrm{wu}}$ in a ramp shape over 100 ms, causing the active power flow from WPPs to Rec1. It resulted in the increase of i_{Rec1} according to the dc current control with reference to the active power. The recovered Line1 was charged during this time. The charging current corresponds to the difference of the currents between the sending end and the receiving end, which are i_{Rec1} and i_{Line1}, respectively. When the voltage of Line1 v_{Line1} reached 1 pu at $t = 0.15$ s, the system started the power transmission through the recovered Line1. The cell capacitor voltages of Rec1 v_{u8}, v_{v8}, v_{w8}, v_{u16}, v_{v16}, v_{w16} were balanced well during this operation.

Before the system switching ($t < 0$ s), the current of Line1 i_{Line1} was 0 pu, and the current of Line2 i_{Line2} was 2 pu. This is because both WPP1 and WPP2 were connected to Line2. After the system switching ($t > 220$ ms), i_{Line1} increased to 1 pu whereas i_{Line2} decreased to 1 pu. This result demonstrates that the power transmission of 1 pu on line2 was transferred to Line1 by the system switching in 0.22 s. The state after this system switching is the same as the initial state of the experiment in the Section V-A.

4) Comparison With the FRT Requirement (Y1–Y3): Fig. 16 shows the comparison of V_{FRT} and V_{ac1}. The voltage sag satisfies the range for continuous operation in the FRT requirements. Therefore, the WPPs will be able to continue their operation against the voltage sag and power transmission can be recovered in 0.22 s.

VI. Conclusion

The multicircuit HVDC system can perform fault clearing without dc circuit breakers. However, the existing method requires the shutdown of the WPPs connected to the faulted line. Thus, the power transmission suspends until restarting the WPPs. This article has proposed the system switching method that enables the continuous operation of the WPPs under the dc line fault. It intentionally generates a voltage sag in the power plants during fault clearance and system switching to decouple the ac and dc current. The voltage sag is designed to meet the FRT requirement for the WPPs. Therefore, the WPPs can achieve continuous operation during the system switching. This article has also proposed the switching method in normal operation after recovering the faulted line. It enables to return to the initial state before the fault while continuing the operation of WPPs. The validity of the proposed method was verified by the experimental HVDC system rated at 11 kW. The experiment confirmed the continuous operation of the WPPs under both a dc pole-to-ground fault and in the normal operation. The resuming time was 0.2 s under a dc pole-to-ground fault and 0.22 s in the normal operation. Therefore, the proposed method contributes to improve the supply reliability of the multicircuit HVDC system.

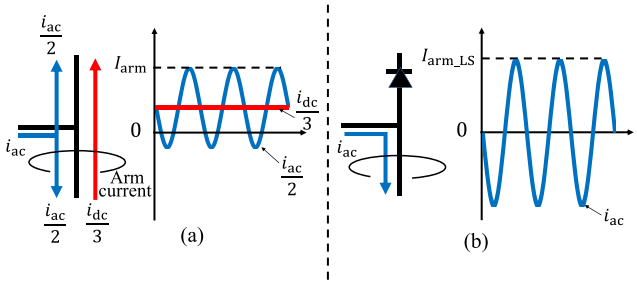

Fig. 17 Arm current during (a) normal operation and (b) lower arm short protection.

APPENDIX A
ARM CURRENT WHILE LOWER ARM SHORT PROTECTION

This section derives the arm current while the lower arm short protection. While the lower arm short protection, the current from the WPP only flows through the lower arm of the rectifier, resulting in an increase of the current amplitude from normal operation. The arm current can be calculated as following steps. While the normal operation of the rectifier, its ac input power is almost equal to its dc output power. Therefore, the following formula holds at rated power operation:

$$\sqrt{3}V_{\rm ac}I_{\rm ac} = V_{\rm dc}I_{\rm dc}$$

$V_{\rm ac}$ and $I_{\rm ac}$ are rated ac line-to-line voltage and ac current, respectively, and $V_{\rm dc}$ and $I_{\rm dc}$ are rated dc voltage and dc current, respectively. While the normal operation, half of the ac current and one-third of the dc current flow in the upper and lower arms as shown in the Fig. 17(a). Therefore, the peak value of the arm current $I_{\rm arm}$ while normal operation can be derived as follows:

$$I_{\rm arm} = \frac{\sqrt{2}I_{\rm ac}}{2} + \frac{I_{\rm dc}}{3} = I_{\rm ac}\left(\frac{\sqrt{2}}{2} + \frac{\sqrt{3}}{3}\frac{V_{\rm ac}}{V_{\rm dc}}\right)$$
$$= I_{\rm ac}\left(\frac{\sqrt{2}}{2} + \frac{\alpha}{2\sqrt{2}}\right)$$

where $\alpha = (2\sqrt{2}/\sqrt{3})(V_{\rm ac}/V_{\rm dc})$ is modulation index. While the lower arm short protection, all the ac current flows in the lower arm in the steady state as shown in the Fig. 17(b). Therefore, the amplitude of the arm current $I_{\rm arm\_LS}$ while lower arm short protection can be derived as follows:

$$I_{\rm arm\_LS} = \beta\sqrt{2}I_{\rm ac}.$$

β represents the ratio of the current supplied by the grid-tied converter during the lower arm short protection to the rated value. Finally, the ratio of the arm current amplitude while the lower arm short protection to the rated value can be derived as follows:

$$\gamma = \frac{I_{\rm arm\_LS}}{I_{\rm arm}} = \frac{\beta\sqrt{2}I_{\rm ac}}{\left(\frac{\sqrt{2}}{2} + \frac{\alpha}{2\sqrt{2}}\right)I_{\rm ac}} = \frac{4\beta}{2+\alpha}. \quad (1)$$

The experimental setup was designed to be $\alpha = 0.96$ and $\beta = 1.2$. Substituting them to (1) yields $\gamma = 1.62$. The lower arms should be designed to withstand the current.

However, the γ can be decreased without additional components. β can be reduced to be 1 or less in reality by modifying the current control of the grid-tied converter. If β is changed from 1.2 to 1, then γ becomes 1.35. Furthermore, β becomes almost zero if the grid-tied converter is controlled to supply no current when the short circuit occurs. In this condition, γ becomes zero, which means the arm current no longer flows during the lower arm short protection in the steady state. Furthermore, injecting third order zero sequence component to the arm voltage at the rectifier improves the modulation index α up to 1.15, and it also decreases γ. In conclusion, γ becomes 1.35–1.62 in the existing method, however it can be much decreased by the controls without additional components.

REFERENCES

[1] Working Group B4.55, "HVDC connection of offshore wind power plants," CIGRE, Tech., Brochure 619, May 2015.

[2] V. Hussennether et al., "Projects BorWin2 and HelWin1– large scale multilevel voltage-sourced converter technology for bundling of offshore windpower," CIGRE Session B4-306, 2012.

[3] W. Leterme, I. Jahn, P. Ruffing, K. Sharifabadi, and D. Van Hertem, "Designing for high-voltage dc grid protection: Fault clearing strategies and protection algorithms," *IEEE Power Energy Mag.*, vol. 17, no. 3, pp. 73–81, May/Jun. 2019.

[4] S. H. Ashrafi Niaki, Z. Liu, Z. Chen, B. Bak-Jensen, and S. Hu, "Protection system of multi-terminal MMC-based HVDC grids: A survey," in *Proc. IEEE Int. Conf. Power Energy Syst. Appl.*, 2022, pp. 167–177.

[5] T. Senda, T. Tamagawa, K. Higuchi, T. Horiuchi, and S. Yanabu, "Development of HVDC circuit breaker based on hybrid interruption scheme," *IEEE Trans. Power App. Syst.*, vol. PAS-103, no. 3, pp. 545–552, Mar. 1984.

[6] T. Eriksson, M. Backman, and S. Halen, "A low loss mechanical HVDC breaker for HVDC grid applications," in *Proc. CIGRE Session*, 2014, pp. 1–8.

[7] D. Jovcic and B. Wu, "Fast fault current interruption on high-power DC networks," in *IEEE PES Gen. Meeting*, 2010, pp. 1–6.

[8] K. Sano and M. Takasaki, "A surgeless solid-state DC circuit breaker for voltage-source-converter-based HVDC systems," *IEEE Trans. Ind. Appl.*, vol. 50, no. 4, pp. 2690–2699, Jul./Aug. 2014.

[9] M. Callavik, A. Blomberg, J. Häfner, and B. Jacobson, "The hybrid HVDC breaker, an innovation breakthrough enabling reliable HVDC grids," *ABB Grid Syst.*, Zürich, Switzerland, Tech. Paper, Nov. 2012.

[10] W. Zhou et al., "Development and test of a 200 kV full-bridge based hybrid HVDC breaker," *Proc. IEEE 17th Eur. Conf. Power Electron. Appl.*, 2015, pp. 1–7.

[11] X. Zhang et al., "A state-of-the-art 500-kV hybrid circuit breaker for a dc grid: The world's largest capacity high-voltage DC circuit breaker," *IEEE Ind. Electron. Mag.*, vol. 14, no. 2, pp. 15–27, Jun. 2020.

[12] H. Pang and X. Wei, "Research on key technology and equipment for zhangbei 500 kV DC grid," in *Proc. IEEE Int. Power Electron. Conf.*, 2018, pp. 2343–2351.

[13] C. Meyer, M. Kowal, and R. W. D. Doncker, "Circuit breaker concepts for future high-power DC-applications," in *Proc. IEEE 40th IAS Annu. Meeting. Conf. Rec. Ind. Appl. Conf.*, 2005, pp. 860–866.

[14] F. Mohammadi et al., "HVDC circuit breakers: A comprehensive review," *IEEE Trans. Power Electron.*, vol. 36, no. 12, pp. 13726–13739, Dec. 2021.

[15] D. Jovcic, G. Tang, and H. Pang, "Adopting circuit breakers for high-voltage DC networks: Appropriating the vast advantages of DC transmission grids," *IEEE Power Energy Mag.*, vol. 17, no. 3, pp. 82–93, May/Jun. 2019.

[16] L. Tang and B. Ooi, "Locating and isolating DC faults in multi-terminal DC systems," *IEEE Trans. Power Del.*, vol. 22, no. 3, pp. 1877–1884, Jul. 2007.

[17] S. Cui and S. -K. Sul, "A comprehensive DC short-circuit fault ride through strategy of hybrid modular multilevel converters (MMCs) for overhead line transmission," *IEEE Trans. Power Electron.*, vol. 31, no. 11, pp. 7780–7796, Nov. 2016.

[18] E. Shahriari, F. Gruson, P. Vermeersch, P. Delarue, F. Colas, and X. Guillaud, "A novel DC fault ride through control methodology for hybrid modular multilevel converters in HVDC systems," *IEEE Trans. Power Del.*, vol. 35, no. 6, pp. 2831–2840, Dec. 2020.
[19] R. Marquardt, "Modular multilevel converter topologies with DC-Short circuit current limitation," in *Proc. IEEE 8th Int. Conf. Power Electron. - ECCE Asia*, 2011, pp. 1425–1431.
[20] A. A. Elserougi, A. M. Massoud, and S. Ahmed, "A switched-capacitor submodule for modular multilevel HVDC converters with DC-Fault blocking capability and a reduced number of sensors," *IEEE Trans. Power Del.*, vol. 31, no. 1, pp. 313–322, Feb. 2016.
[21] X. Li, W. Liu, Q. Song, H. Rao, and S. Xu, "An enhanced MMC topology with DC fault ride-through capability," in *Proc. IEEE 39th Annu. Conf. Ind. Electron. Soc.*, 2013, pp. 6182–6188.
[22] J. Qin, M. Saeedifard, A. Rockhill, and R. Zhou, "Hybrid design of modular multilevel converters for HVDC systems based on various submodule circuits," *IEEE Trans. Power Del.*, vol. 30, no. 1, pp. 385–394, Feb. 2015.
[23] K. Sano, "A concept of multi-circuit HVDC transmission system for selective fault clearing without DC circuit breakers," in *Proc. IEEE Int. Conf. Smart Grids Energy Syst.*, 2020, pp. 431–436.
[24] M. Enomoto, K. Sano, J. Kanno, and J. Fukushima, "Continuous operation of wind power plants under DC line faults in multi-circuit HVDC transmission system," in *Proc. IEEE Energy Convers. Congr. Expo.*, 2021, pp. 1236–1240.
[25] P. Bresesti, W. L. Kling, R. L. Hendriks, and R. Vailati, "HVDC connection of offshore wind farms to the transmission system," *IEEE Trans. Energy Convers.*, vol. 22, no. 1, pp. 37–43, Mar. 2007.
[26] G. Tang and Z. Xu, "A LCC and MMC hybrid HVDC topology with dc line fault clearance capability," *Int. J. Elect. Power Energy Syst.*, vol. 62, pp. 419–428, Nov. 2014.
[27] M. Andersson, X. Yang, and C. Yuan, "2-terminal hybrid HVDC cost effective alternatives for clearing temporary dc line faults," in *Proc. IEEE PES Asia-Pacific Power Energy Eng. Conf.*, 2017, pp. 1–6.
[28] N. M. Haleem, A. D. Rajapakse, A. M. Gole, and I. T. Fernando, "Investigation of fault ride-through capability of hybrid VSC-LCC multi-terminal HVDC transmission systems," *IEEE Trans. Power Del.*, vol. 34, no. 1, pp. 241–250, Feb. 2019.
[29] M. Wang, W. Leterme, G. Chaffey, J. Beerten, and D. Van Hertem, "Pole rebalancing methods for pole-to-ground faults in symmetrical monopolar HVDC grids," *IEEE Trans. Power Del.*, vol. 34, no. 1, pp. 188–197, Feb. 2019.
[30] F. Blaabjerg and K. Ma, "Wind energy systems," *Proc. IEEE*, vol. 105, no. 11, pp. 2116–2131, Nov. 2017.
[31] K. Sano and H. Nakayama, "A fault protection method for avoiding overvoltage in symmetrical monopole HVDC systems by half-bridge MMC," *IEEE Access*, vol. 9, pp. 165219–165226, 2021.
[32] ABB's high voltage cable unit, "XLPE submarine cable systems: Attachment to XLPE land cable systems-users guide," Rev. 5. Accessed: Dec. 1, 2022. [Online]. Available: https://new.abb.com/docs/default-source/ewea-doc/xlpe-submarine-cable-systems-2gm5007.pdf
[33] The Japan Electric Association, "Grid-interconnection code," JEAC 9701-2019, 2019.

Mitsuyoshi Enomoto (Student Member, IEEE) received the B.S. and M.S. degrees in electrical and electronic engineering, in 2020 and 2022, respectively, from Tokyo Institute of Technology, Tokyo, Japan, where he is currently working toward the Ph.D. degree in electrical and electronic Engineering.

His research interest includes HVDC transmission system.

Kenichiro Sano (Member, IEEE) received the B.S. degree in international development engineering, and the M.S. and Ph.D. degrees in electrical and electronic engineering from the Tokyo Institute of Technology, Tokyo, Japan, in 2005, 2007, and 2010, respectively.

From 2008 to 2010, he was a JSPS Research Fellow. In 2008, he was a Visiting Scholar with the Virginia Polytechnic Institute and State University, Blacksburg, VA, USA. From 2010 to 2018, he was a Research Scientist with the Central Research Institute of Electric Power Industry (CRIEPI) in Japan. In 2018, he joined the Tokyo Institute of Technology, where he is currently an Assistant Professor with the Department of Electrical and Electronic Engineering. His current research interests include power electronics for utility applications, high-voltage dc transmission systems, and power system quality.

Junya Kanno received the M.S. and Ph.D. degrees in electrical and electronic Engineering from Meiji University, Tokyo, Japan, in 1992, and 1997, respectively.

In 1992, he joined the Tokyo Electric Power Company (TEPCO), Japan, where he is currently the Senior Researcher with R&D Department, TEPCO Research Institute. His research interests include power electronics, HVDC transmission system, and photovoltaic power generation.

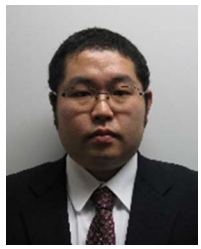

Junichi Fukushima received the M.S. degree in electrical and electronic engineering from Seikei University, Tokyo, Japan, in 2010.

In 2010, he joined the Tokyo Electric Power Company (TEPCO), where he was engaged in planning and operation of hydroelectric power plants and substations. He is currently the Researcher with R&D Department, TEPCO Research Institute. His research interests include power electronics and HVDC transmission system.